Optimum discrete location of a shape memory alloy wire for discrete actuation of a compliant link

ARTICLE *in* JOURNAL OF MECHANICAL DESIGN · FEBRUARY 2010

Impact Factor: 1.25 · DOI: 10.1115/1.4000643

3 AUTHORS:

Atanu Banerjee
Indian Institute of Technology Guwahati
10 PUBLICATIONS **60** CITATIONS
SEE PROFILE

Bishakh Bhattacharya
Indian Institute of Technology Kanpur
62 PUBLICATIONS **150** CITATIONS
SEE PROFILE

A. K. Mallik
Indian Institute of Engineering Science and T…
83 PUBLICATIONS **1,085** CITATIONS
SEE PROFILE

Optimum Discrete Location of Shape Memory Alloy Wire for Enhanced Actuation of a Compliant Link

A. Banerjee
Research Scholar

B. Bhattacharya
Associate Professor

A. K. Mallik
Professor

Department of Mechanical Engineering,
IIT Kanpur,
Uttar Pradesh 208016, India

For discrete actuation with shape memory alloy (SMA) wires, the actuation moment can be controlled by changing the amount of wire offset. Increasing offset not only enhances the actuating moment, but also demands larger displacement capability of the actuator. In this paper, large deflection of a cantilever beam actuated by a SMA wire has been investigated. Both the theoretical and experimental results reveal the existence of an optimum offset maximizing the end deflection. The optimum offset depends on the flexural stiffness of the beam, SMA wire properties, and the input actuation level.
[DOI: 10.1115/1.4000643]

1 Introduction

Shape memory alloys (SMAs) have many attractive mechanical properties such as shape memory effect (SME), which renders them suitable as actuators. The large recovery stress of the order of 1 GPa and large recoverable strain (6–8%) capability of SMAs make them superior over other smart materials. SMA is available mainly in the form of wires, stripes, coils, etc., out of which the wire form is mostly used as actuators. During the past few decades a lot of researches had been carried out designing SMA based actuators [1]. These are used for navigation of dead weights, manipulation of robotic arms [2], shape control of aerodynamic profile [3], actuation of biomimetic prosthetic hand [4], and single or multiple link compliant mechanisms [5]. In these applications, SMA wires are either embedded in the structure [3] to make a composite or used discretely. In case of discrete actuation, the SMA wire is kept with an offset to the host and attached to it at some discrete points. For most of the applications, it is desirable that SMA wires are used to produce the maximum possible actuating forces or moments. For example, the workspace of a flexible manipulator or a compliant mechanism can be enlarged by enhancing the actuation capability of SMA wires. To obtain enhanced actuation, a number of configurations for discrete actuation have been proposed in literature [6]. However, the effect of variation in the offset has not been addressed. In this paper, large deflection of an elastic cantilever beam (model of a compliant link) discretely actuated using a SMA wire with varying offset has been analyzed. The results show the presence of an optimum offset maximizing the end deflection. The variation of the optimum offset with different parameters, such as flexural rigidity of the beam, SMA wire properties, and the maximum actuation temperature, has been investigated. Experimental results are shown to validate the theory. Based on these, an empirical formula is suggested for the optimum offset as a function of the flexural rigidity of the host and the maximum actuation temperature of the SMA.

The purpose of keeping the actuator discrete to the host is to enhance the actuating moment by increasing the distance between the line of application of the force and the neutral plane of bending. The resulting enhanced actuation can only be obtained if the actuator is capable of undergoing the associated extra amount of displacement. This can be better understood from Fig. 1, which shows a deflected beam element XYZ under a force applied along either AA' or BB'. BX and $B'Z$ are the rigid elements connected perpendicularly to the beam element XYZ to provide the desired offset. It is obvious that in order to achieve the same deformed configuration of the beam, the force required along BB' is less compared with that along AA'. Simultaneously, the displacement requirement along BB' is higher compared with that in AA' as $BB' < AA'$. Since every smart material has its own actuation capability (force-displacement relation), there will be a particular offset above which the displacement capability is exhausted prior to saturation of the actuation force and below that, the actuation force gets saturated before the full exploitation of the maximum displacement capability. Furthermore, for a given temperature, the maximum force and displacement capabilities of these SMA actuators depend on the bending stiffness of the host as well. Therefore, due to the complicated interaction between the host and the actuator, an optimum offset exists providing the maximum deformation of the host for the same input actuation.

Theoretical simulation of the problem involves constrained recovery of the SMA wire, which has been attempted by many researchers [6,7]. The analysis needs consideration of thermomechanical constitutive relation of the SMA wire, the equilibrium of the host structure, and the kinematic constraint between the structure and the SMA. Large deflection of a cantilever beam has been modeled using Euler–Bernoulli moment-curvature relationship taking into consideration the effect of the end moment as well as the end forces. This mechanical analysis has been kinematically coupled with the thermomechanical constitutive (1D Brinson model) relation of the SMA wire.

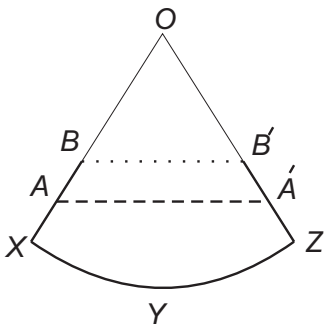

Fig. 1 Deformed beam element under discrete actuation

Contributed by the Design Innovation and Devices Committee of ASME for publication in the JOURNAL OF MECHANICAL DESIGN. Manuscript received January 27, 2009; final manuscript received September 24, 2009; published online January 14, 2010. Assoc. Editor: Diann Brei.

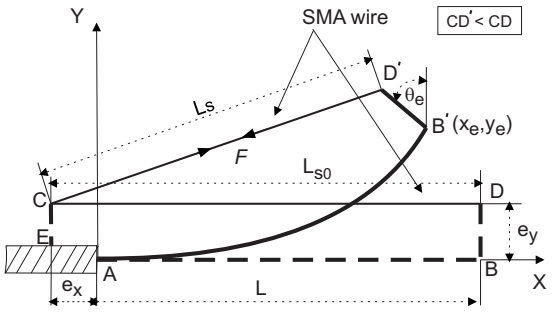

Fig. 2 A deformed cantilever beam due to discrete actuation using a SMA wire

2 Analysis of Large Deflection of a Cantilever Beam

In this section, large deflection of a cantilever beam has been modeled under the follower forces exerted by the SMA wire, discretely attached to it. In Fig. 2, AB is the undeformed configuration (dashed) of a cantilever beam with an attached SMA wire CD at an offset e_y. As the temperature is increased, the SMA wire contracts, $(L_s < L_{s0})$ thus resulting in the deformed configuration of the beam AB'. The connectors BD and CE are assumed to be rigid and are always perpendicular to the neutral plane of the beam. The end point coordinates of the beam are (x_e, y_e) and the end slope is θ_0. Figure 3 shows the deflected shape of the beam under end moments and forces acting on it.

2.1 Analytical Approach. Considering only the effect of the end moment M_0 and using the Euler–Bernoulli moment-curvature relationship one can obtain

$$\frac{d\theta}{ds} = \frac{M_0}{EI} = C \quad \text{(say)} \tag{1}$$

where EI is the flexural rigidity of the beam and $d\theta/ds$ is the curvature with θ as the slope at the point of interest, which is at a distance s measured along the arc of the bent beam. The moment can be written as $M_0 = Fe_y = \sigma A e_y$ where σ is the induced stress within the SMA wire having area of cross-section A. The change in the angle between the SMA wire and the rigid support BD' has been neglected. Integrating Eq. (1) and using the boundary condition (B.C.) $\theta_{s=0} = 0$, the final form can be obtained as $\theta(s) = Cs$. The expressions for $x(s)$ and $y(s)$ can be obtained integrating $dx/ds = \cos\theta(s)$ and $dy/ds = \sin\theta(s)$, respectively. Using the B.C.s as $x_{s=0} = 0$ and $y_{s=0} = 0$ one can get $x(s) = \sin Cs/C$ and $y(s) = (1 - \cos Cs)/C$, respectively. The coordinates of the free end of the beam can be written as

$$x_e = \frac{\sin\kappa}{C} \quad \text{and} \quad y_e = \frac{(1-\cos\kappa)}{C} \tag{2}$$

where $\kappa = CL$ and L is the length of the beam. The coordinates of the point D' in Fig. 2 are obtained as $x_D = (1/c - e_y)\sin\kappa$ and $y_D = ((1-\cos\kappa)/C + e_y\cos\kappa)$. Thus, the length of the SMA wire in the deformed configuration of the beam is obtained as

$$L_s = \{(x_D + e_x)^2 + (y_D - e_y)^2\}^{1/2} = \left\{ e_x^2 + 2\sin\kappa\left(\frac{1}{c} - e_y\right)e_x + 2\left(\frac{1}{c} - e_y\right)^2(1-\cos\kappa)\right\}^{1/2} \tag{3}$$

For $e_x = 0$, Eq. (3) takes the form $L_s = 2(1/C - e_y)\sin\kappa/2$. If ε_0 is the initial strain within the SMA wire, then the initial length of the prestrained SMA wire can be written as $L_{s0} = L_0(1+\varepsilon_0)$, where L_0 is the length of the unstretched wire and the present strain can be expressed as

$$\varepsilon = \left(\frac{L_s - L_0}{L_0}\right) = \left\{\frac{L_s(1+\varepsilon_0)}{L_{s0}} - 1\right\} \tag{4}$$

Thus, for a given stress, the coordinates of the free end of the beam and the strain within the SMA wire can be obtained using Eqs. (2)–(4).

2.2 Numerical Approach. In the above analytical derivation, only the effect of the end moment has been considered. Including the effect of end forces, the bending moment at any point (x, y) of the beam can be written as

$$M(x(s), y(s)) = M_0 + F_h(y_e - y(s)) - F_v(x_e - x(s)) \tag{5}$$

where $M_0 = Fe_y\cos(\theta_0 - \alpha)$, $F_h = F\cos\alpha$, and $F_v = F\sin\alpha$. All the angles are indicated in Fig. 2. It can be noted that the magnitudes of the forces are dependent on the deformed shape of the beam; i.e., these are follower forces. Neglecting the axial deformation of the beam and using Euler–Bernoulli beam theory, the deflected configuration of the beam can be obtained by solving the following set of coupled nonlinear ordinary differential equations (ODEs):

$$\frac{d\theta}{ds} = \frac{F}{EI}\{e_y\cos(\theta_0 - \alpha) + (y_e - y(s))\cos\alpha - (x_e - x(s))\sin\alpha\}$$

$$\frac{dx}{ds} = \cos\theta(s) \tag{6}$$

$$\frac{dy}{ds} = \sin\theta(s)$$

with the following set of initial conditions:

$$\theta_{s=0} = 0$$

$$x_{s=0} = 0 \tag{7}$$

$$y_{s=0} = 0$$

2.2.1 Algorithm for Beam Analysis. Initially $x(s)$, $y(s)$, $\theta(s)$, x_e, y_e, θ_0, and α are assumed to be zero.

For a given force in the SMA wire, the end forces F_h and F_v and the end moment M_0 are determined.

The set of ODEs in Eq. (6) is numerically integrated using the initial conditions given by Eq. (7).

The values of $x(s)$, $y(s)$, $\theta(s)$, x_e, y_e, and θ_0 are updated.

The angle α is obtained using $\tan\alpha = (y_e - e_y(1-\cos\theta_0))/(x_e + e_x - e_y\sin\theta_0)$.

The difference between the two configurations is obtained as

$$\Delta = \sum\{(\theta(s)_{\text{old}} - \theta(s)_{\text{new}})^2 + (x(s)_{\text{old}} - x(s)_{\text{new}})^2 + (y(s)_{\text{old}} - y(s)_{\text{new}})^2\}^{1/2}$$

If $\Delta > 10^{-10}$, the program returns to step (3) with the new values of $x(s)$, $y(s)$, $\theta(s)$, x_e, y_e, θ_0, and α.

Else the program terminates and the strain in the SMA wire is obtained (following the approach described in Sec. 2.1) using the

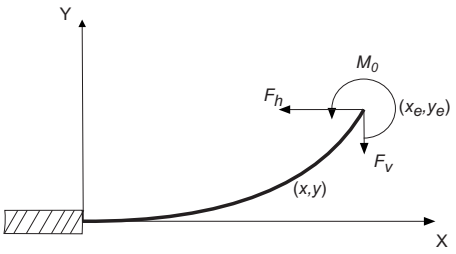

Fig. 3 End forces and moments applied on the beam by the SMA wire

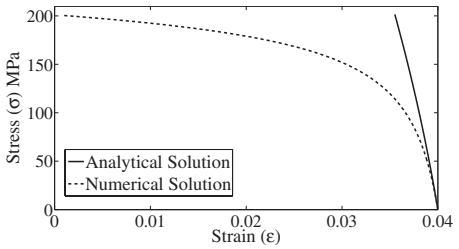

Fig. 4 Stress strain relation of the SMA obtained using the two analyses

final values of x_e, y_e, θ_0, and α.

While modeling constrained recovery of a SMA, only the effect of the end moment, which too under approximations is discussed in Sec. 2.1, is normally considered. The stress-strain relationship for a SMA wire, when connected to a particular beam with a given offset, can be obtained using the two approaches mentioned above. Numerical results obtained with e_y=2.0 mm and ε_0 =0.04 for Beam-3 listed in Table 2 (see Sec. 5) are shown in Fig. 4. The huge difference between the two results clearly establishes the importance of the numerical approach including the effect of end forces. Consequently numerical approach has been used in the rest of this work.

3 Modeling of Shape Memory Alloy

Among the smart materials, the SMA draws considerable attention of the researchers due to its large strain (6–8%) capability. Once deformed mechanically at low temperature, it can completely recover the strain upon heating above a critical temperature called the austenite finish temperature. This is called the SME. This property makes the SMA suitable for actuation purposes. Drawing the SMA wire isothermally above austenite finish temperature, after a critical value of stress, large strain can be obtained with nearly a constant load, which in turn can be completely recovered upon unloading with a large hysteresis. This phenomenon is called *pseudo-elasticity* (PE) or *superelasticity* (SE). This effect finds application in energy dissipating structures. All these phenomena emerge from the crystallographic change in SMA due to thermal and/or mechanical loading [8–10]. With loading at a temperature lower than the martensite finish temperature, the multiple variants of martensite (product phase) get converted to a single variant martensite (detwinned martensite); orientation of which depends on the Schmidt factor and crystallographic directions of the SMA [9]. This is termed as detwinning. Upon unloading, an apparent permanent strain sets in, which is fully recoverable upon heating (above the austenite finish temperature) followed by cooling in the absence of any stress resulting in a twinned martensite (SME). In PE or SE, the austenite directly gets converted to a detwinned martensite while loading and austenite form is regained upon unloading. In this process it exhibits a hysteresis. All these phenomena can be shown through the stress-temperature diagram called the phase diagram of the SMA. A typical phase diagram is shown in Fig. 5. M_s, M_f, A_s, and A_f are, respectively, the martensite start, martensite finish, austenite start, and austenite finish temperature at zero stress. σ_s^{cr} and σ_f^{cr} are, respectively, the stress values corresponding to which the stress induced transformation (detwinning) starts and ends. C_a and C_m are the slopes describing how the transformation temperatures change with induced stress. Though the variations of critical temperatures with stress are nonlinear in nature, for the sake of simplification of analysis a linear variation is assumed. The experimental procedures involved in determining these properties can be found in Ref. [11].

For the past few decades researchers are involved in developing a constitutive relationship capable of describing the SME and SE. There are mainly three approaches: (a) phenomenological approach, (b) continuum mechanics based approach, and (c) microstructure based model. The phenomenological model, based on thermomechanics and experimentally obtained kinetics of phase change, was first developed by Tanaka [10]. In this model, the temperature, stress, and martensite volume fraction are taken as the state variables. The change in the martensite volume fraction with temperature is obtained through curve fitting of the experimental data and is found to be exponential. Liang and Rogers [12] proposed a rate form of the constitutive model of Tanaka [10] and used a cosine model for the phase kinetics. In both these approaches, the twinned and detwinned martensite phase fractions are not distinguished. As a result, these models are unable to capture the detwinning phenomena, the main reason behind the shape memory effect. Brinson [13] introduced two different volume fractions of twinned and detwinned martensites and thus removing the deficiencies of the previous models. This model is used for most of the applications of SMA. The other two approaches, based on thermodynamics principle, are derived from free energy and dissipation potential. For more information regarding modeling and applications of SMA one should refer to Ref. [14]. In the present work, the 1D phenomenological model with nonconstant material parameters proposed by Brinson [13] has been used.

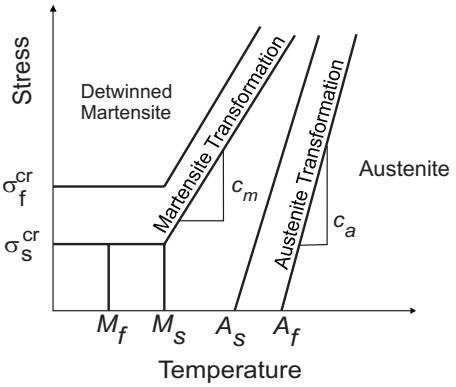

Fig. 5 Typical phase diagram of the shape memory alloy

3.1 1D Constitutive Model (Brinson Model). The integrated form of the constitutive law relates stress (σ), strain (ε), temperature (T), and volume fraction of the detwinned martensite (ξ_s) as [13]

$$\sigma - \sigma_0 = D(\xi)\varepsilon - D(\xi_0)\varepsilon_0 + \Omega(\xi)\xi_s - \Omega(\xi_0)\xi_{s0} + \Theta(T - T_0) \tag{8}$$

where $D(\xi)$ is the elastic modulus, $\Omega(\xi)$ is the transformation modulus, Θ is related to the thermal expansion coefficient, and subscript $(.)_0$ refers to the initial state of the SMA. $D(\xi)$ is calculated using $D(\xi)=\xi D_m+(1-\xi)D_a$, where D_m and D_a are the elastic moduli corresponding to fully martensite and fully austenite states. $\Omega(\xi)$ is obtained using the relation $\Omega(\xi)=-\varepsilon_L D(\xi)$, where ε_L is the maximum reversible strain possible. The total martensite volume fraction $\xi=\xi_t+\xi_s$, where ξ_s and ξ_t are, respectively, the stress and temperature induced martensite volume fractions. The variation of martensite volume fractions with stress and temperature or phase kinetics can be represented as

$$\xi = \xi(\sigma, T) \tag{9}$$

The functional forms of these variations presented in Eqs. (22a)–(23b) of Ref. [13] are used in this work.

4 Solution Algorithm

The strain (ε) is a function of stress (σ) in the SMA wire and is determined using the analysis presented in Sec. 2.2.

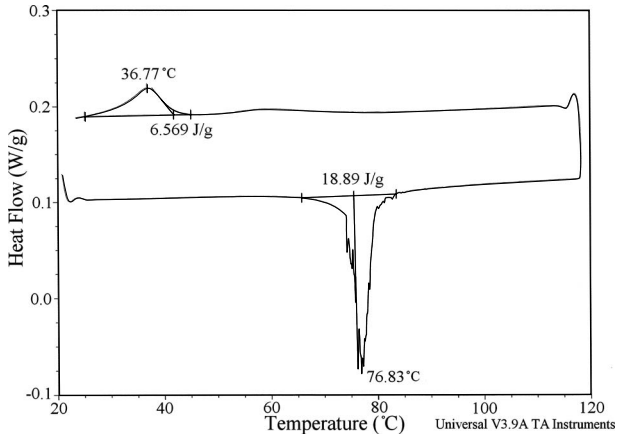

Fig. 6 Transformation temperatures of the SMA wire obtained from the DSC experiment

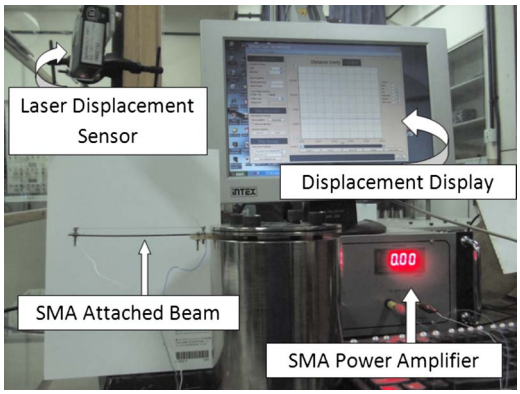

Fig. 7 Detailed experimental setup

The phase kinetics relations proposed by Brinson [13] are used to compute martensite volume fractions (ξ, ξ_s) for a given stress (σ) and temperature (T).

For a given temperature (T) the constitutive equation (8) becomes nonlinear with stress (σ) as the only unknown.

For a given temperature increment, Eq. (8) is solved using golden-section search method to determine the corresponding stress in the SMA wire.

Because of the nonlinearity, the solution depends on the step size (temperature increment). Here 0.1°C has been chosen as the step size.

The SMA wire temperature has been increased up to a final value, which is termed as the *maximum actuation temperature*, and the end deflection of the beam corresponding to this temperature is noted.

5 Experimental Details

The SMA wire used is Flexinol HT 125 μm obtained from Dynalloy, CA. The properties of the SMA wire are enlisted in Table 1. The transformation temperatures at zero stress are determined experimentally using differential scanning calorimetry (DSC) as shown in Fig. 6. The SMA is heated above the austenite finish temperature to determine the amount of prestrain, which is found to be ~4%. Other properties of the SMA are taken from literature [13]. Experiments are conducted on three beams having different flexural stiffnesses, the details of which are given in Table 2. In each of the beams a connector screw is attached at the free end. The SMA wire is fastened with the connector screw as shown in Fig. 7. The other end of the SMA is held using a similar screw connector fixed to the rigid support, where the beam is clamped as shown in Figs. 7 and 8. The offset of the SMA wire is changed by rotating the screw. The length of the cantilever beam is 100 mm. The clamped end of the beam is fixed to a massive rigid base. The temperature of the SMA wire is increased using resistive heating by a current from a dc source. As the temperature of the SMA wire is raised to above A_s, recovery stress within the SMA develops resulting in beam deflection. The end deflection of the beam is noted continuously using a "Micro-Epsilon" (Germany) laser sensor until it reaches the maximum value. The SMA is then cooled gradually by reducing the voltage to zero and allowing natural convection. During cooling, the force exerted by the deformed beam initiates stress induced transformation in the SMA; thus the beam almost comes back to its initial undeformed configuration.

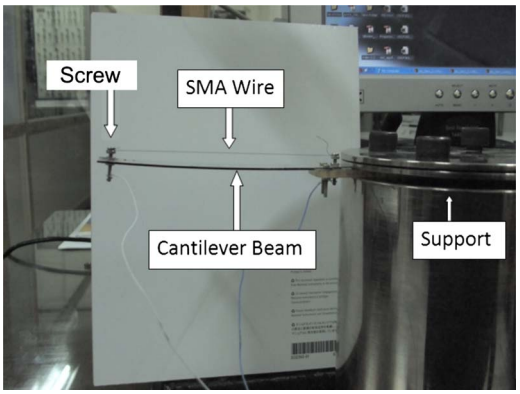

Fig. 8 SMA attached cantilever beam (experimental setup)

The end deflection of Beam-3 for a given offset is shown in Fig. 9 for 5 cycles, where each cycle consists of heating the SMA wire followed by cooling. It can be observed that at the end of every cycle, the beam does not completely recover its initial undeformed state. This is possibly because the final stress value in the SMA wire after each cycle is inadequate for stress induced transformation. Thus the initial strain in the SMA wire changes with changing offset values. Though the change in the strain value is negligible, the accumulation of these small changes can make a significant difference in the SMA wire behavior, if the same wire is used for all offset values. In order to minimize the error, two wires were used. In one, the offset was increased gradually, starting from the lowest value. In the second wire, the offset was gradually reduced from the maximum value. Corresponding to every offset value of a given wire the experiments were conducted for 5 cycles. Thus a total of ten readings are observed for a given

Table 1 Shape memory alloy properties

Moduli	Transformation temperature	Transformation constants	Maximum residual strain: ε_L=0.06
D_a=75 GPa	M_s=44.99°C	C_m=8 MPa/°C	Prestrain: ε_0=0.04
D_m=28 GPa	M_f=25.08°C	C_a=14 MPa/°C	
Θ=0.55 MPa/°C	A_s=65.73°C	σ_s^{cr}=100 MPa	
	A_f=83.50°C	σ_f^{cr}=170 MPa	

Table 2 Beam properties

No.	Beam material	Elastic modulus (GPa)	Beam thickness (mm)	Beam width (mm)	Flexural rigidity (N mm^2)
1	Acrylic	2.38	2.8	11.0	$4.78e^4$
2	Acrylic	2.38	1.8	10.0	$1.16e^4$
3	Acrylic	1.78	1.1	15.5	$3.06e^3$

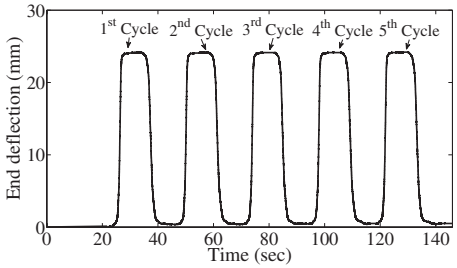

Fig. 9 Experimentally observed end deflection of Beam-3 for multiple cycles

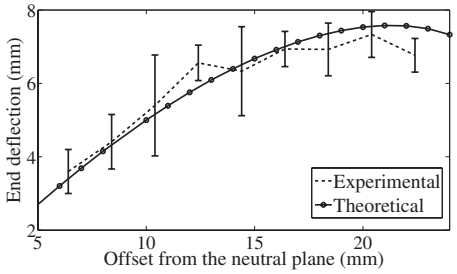

Fig. 10 Maximum end deflections of Beam-1 (in Table 2) for various offset values

offset value. From this set of data the mean and the standard deviation σ_d are calculated. The variation shown in the results corresponds to $\pm\sigma_d$.

6 Results and Discussions

Direct measurement of the temperature of such a fine (125 μm) SMA wire is difficult. Therefore, the maximum actuation temperature is indirectly estimated so as to represent the experimental response of Beam-1 (in Table 2) correctly. Since the input actuation level (voltage) is kept same for all the cases, the same maximum actuation temperature has been used for the rest of the cases. Figure 10 shows the theoretical and experimental end deflections (maximum) of Beam-1 for various offset values. It reveals that the end deflection increases with increasing offset up to a limit beyond which the end deflection decreases with increasing offset. Hence, there is a particular offset (in this case around 20 mm) corresponding to which the maximum deflection is achieved. It can also be observed that the end deflection corresponding to the optimum offset is more than twice of what is obtained with the wire placed near the surface of the host beam.

Similar results for Beam-2 (in Table 2) are shown in Fig. 11. In this case, the optimum offset is around 6 mm. Here also the magnification of the end deflection as compared with the surface actuation is more than by a factor of 2.

The results shown in Figs. 10 and 11 are obtained with the same SMA wire and a given actuation voltage. Prior to the optimum offset, the maximum force capacity of the SMA gets exploited, whereas afterwards the shape memory strain vanishes. This happens because corresponding to the near surface position of the SMA wire, the beams are stiff enough to exploit the force capacity of the SMA wire. However, for a beam having low flexural rigidity, it may happen that the shape memory strain gets exhausted for the near surface position of the SMA. Such a case (Beam-3 in Table 2) is illustrated in Fig. 12, where the near surface location of the SMA wire itself yields maximum deflection.

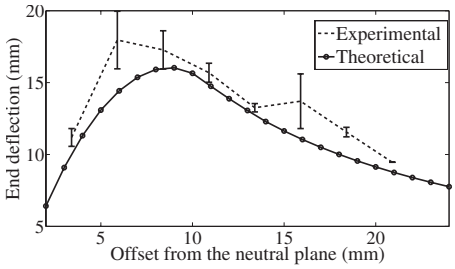

Fig. 11 Maximum end deflections of Beam-2 (in Table 2) for various offset values

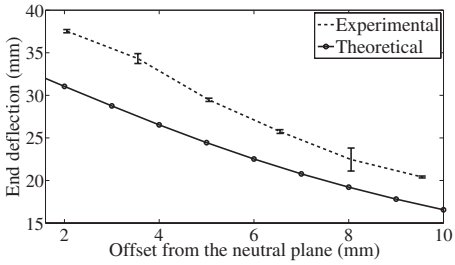

Fig. 12 Maximum end deflections of Beam-3 (in Table 2) for various offset values

From Figs. 10–12 it may be noted that the optimum offset increases with increasing flexural rigidity of the beams for a given SMA wire. This is obvious, because as the beam becomes stiffer, higher bending moment is required, which necessitates a larger offset.

The effect of a constant external load at the free end on the optimum offset is shown in Fig. 13. The modified analysis required in the presence of an end load is described in detail in the Appendix. Experiments have been carried out with different offset values and an external weight of 20 g attached at the end of Beam-2 (in Table 2). Both the theoretical and experimental results suggest that there is a slight increment in the optimum offset value due to the presence of the external load. This is reasonable in the sense that in the presence of the load, the SMA has to exert more moments to lift the load.

The effects of the SMA wire properties on the optimum offset and the maximum end deflection have been studied through simulation. In order to get an idea, the value of C_a is varied for Beam-1

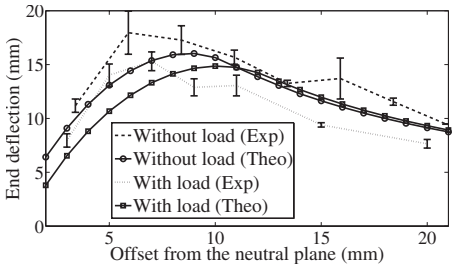

Fig. 13 Effect of external load on the optimum offset of Beam-2 in Table 2

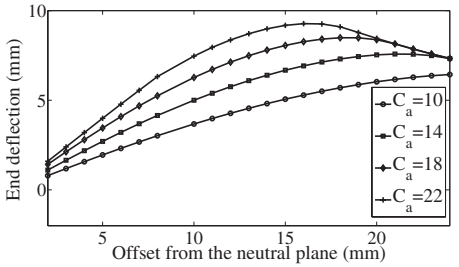

Fig. 14 Maximum end deflections (of Beam-1 in Table 2) for various offset values with different C_a (MPa/°C)

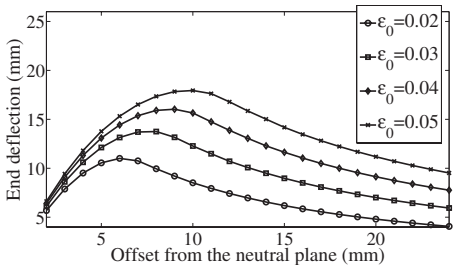

Fig. 15 Maximum end deflections (of Beam-2 in Table 2) for various prestrain values of the SMA

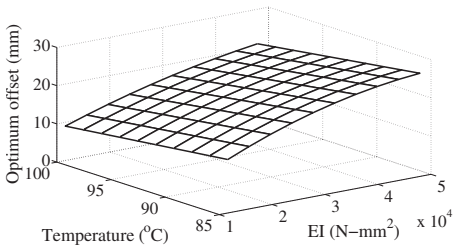

Fig. 16 Optimum offset for different flexural rigidities and actuation temperatures

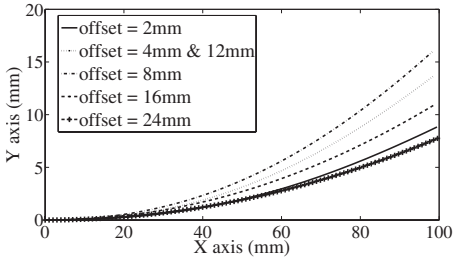

Fig. 17 Deformed beam configurations for different values of offset

and the results are shown in Fig. 14. It is seen that with increasing C_a the optimum offset decreases. This is reasonable because for a given change in temperature, the SMA with a larger C_a can produce higher recovery stress, thus can produce higher bending moment even with a lower offset. The effect of the SMA prestrain is shown in Fig. 15. It reveals that with increasing prestrain, the optimum offset marginally increases for a given host beam. As the offset increases, the stroke requirement of the SMA wire increases (see Fig. 1), which can be taken care of by a larger prestrain in the SMA wire. The maximum end deflection increases considerably with increasing values of both C_a and ε_0.

The most influencing factor is found to be the actuation temperature. Since increase in the actuation temperature changes the force-displacement capacity of the SMA wire, the same analysis has been carried out for different actuation temperatures of the SMA wire and beams with different flexural stiffnesses. The optimum offset has been plotted as a function of these two in Fig. 16. This shows that the optimum offset decreases with increasing SMA wire temperature for a given beam.

The maximum strain recovery in the SMA is obtained when the transformation from $M \rightarrow A$ is complete. Whether the transformation is complete or not depends on the stress and temperature of the SMA. Since we restricted the temperature to a constant value above austenite start temperature, the final value of stress decides whether the transformation is complete or not. For given values of maximum actuation temperature and offset, the final value of the stress in the SMA increases with the bending stiffness of the beam. On the other hand, for a given beam with the same actuation temperature and decreasing offset, the SMA wire needs to apply a higher force to achieve the same deformed configuration. In other words, the maximum stress in the SMA increases either due to increment in the beam stiffness for a given wire offset or due to decrement in the wire offset for a given beam. Hence the completion of transformation is dictated by the beam stiffness and the wire offset for a given maximum actuation temperature. However, if the actuation temperature is increased, the completion of reverse transformation is more likely even in the presence of higher stresses, thereby increasing the strain recovery capability of the SMA. As a result, larger beam deformation can be achieved even with lower offset or stiffer beam by increasing the actuation temperature.

An empirical relation is proposed, relating the optimum offset as a function of flexural rigidity and actuation temperature, as

$$e(T,EI) = f_1(EI) + \frac{(T-85)}{15}(f_2(EI) - f_1(EI)) \tag{10}$$

where $f_1(EI) = -6.84e^{-9}EI^2 + 7.65e^{-4}EI + 6.045$, $f_2(EI) = -3.85e^{-9}EI^2 + 5.59e^{-4}EI + 3.03$, e is the optimum offset of the SMA wire in mm, T is maximum temperature of the SMA wire in °C, and EI is the flexural rigidity of the beam in N mm^2. Though the relationship provided in Eq. (10) is valid for the properties provided in Table 1, similar expression for any SMA wire and host beam combination can be derived following the methodology discussed above.

Until now the end deflection (along the Y axis) of the beam has been considered to show the effect of variation in offset. But in applications such as SMA wire actuated end effectors, the tip slope of the compliant link is of major importance. For SMA driven compliant mechanisms, the deflected shape is of vital importance, since that, in turn, it decides the workspace. The deflected shapes of Beam-2 (in Table 2) are plotted in Fig. 17 for different offset values and a fixed input actuation. The advantage of the optimum offset from all considerations is evident from these plots.

7 Conclusions

The effects of variation in the offset value of SMA wire actuators in case of discrete actuation of beam members have been studied. Theoretical and experimental results show that depending on the SMA and the host properties, there is a particular value of offset for which the maximum deflection of the beam is obtained. It is also revealed that the use of this particular offset value results in 100% increment in the end deflection. This concept will be very useful in case of path generating compliant mechanisms, actuated by discretely placed SMA wire actuators, since the workspace (the region in which the desired point can move) can be considerably enlarged with optimum offset.

Acknowledgment

The authors would like to thank Dr. R.K. Singh and Dr. R. Ramani of DMSRDE, Kanpur, India for their help during the DSC

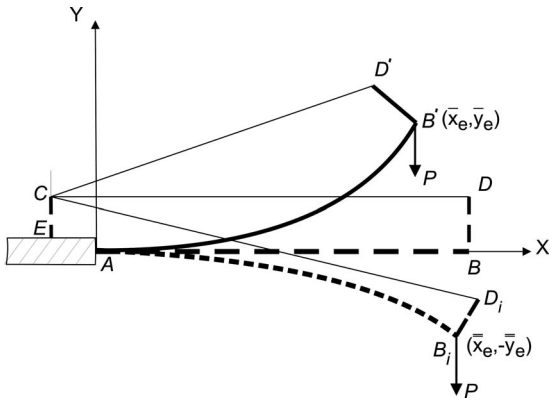

Fig. 18 SMA actuated beam in the presence of external load

experiment and Mr. Jitendra Badothiya for his help in conducting the experiments. The authors would also like to acknowledge the support of the Department of Science and Technology (DST), India under Project No. DST/ME-20060263.

Appendix: Optimum Offset in the Presence of an External Load at the Free End

Referring to Fig. 18, *AB* is the initial undeformed configuration of the beam to which the SMA wire *CD* is attached at a particular offset. Before the thermal activation of the SMA, an external load *P* is applied vertically downwards at the end of the beam. The beam gets deformed to AB_i and therefore the length of the SMA wire is increased to CD_i. Thus, even prior to heating, the wire is subjected to an initial stress. If the induced stress level is more than the stress required to initiate detwinning, then the stress induced martensite volume fraction also increases. Thus, the values of the initial stress, strain, and ξ_s are different from those when there is no external load. In addition, the beam equations also need to be modified slightly to take into account the effect of the external load *P*. The modifications are discussed below.

1 Beam Analysis. In the presence of a constant load *P* acting vertically downwards at the end of the link, Eq. (7) takes the form

$$\frac{d\theta}{ds} = \frac{1}{EI}\{Fe_y \cos(\theta_0 - \alpha) + (y_e - y(s))F\cos\alpha - (x_e - x(s)) \times (F\sin\alpha + P)\}$$

$$\frac{dx}{ds} = \cos\theta(s) \tag{A1}$$

$$\frac{dy}{ds} = \sin\theta(s)$$

Using Eq. (A1) instead of Eq. (7) and following the algorithm stated in Sec. 2.2 the deformed configuration of the beam and the final length of the SMA wire are determined for given values of the stress in the wire and the external load *P*. This analysis enables us to find out the strain in the SMA wire as a function of stress in the presence of the external load.

2 SMA Analysis. The whole thermomechanical process of the SMA consists of two segments. In the first segment, the SMA gets elongated due to the application of the external load. This is an isothermal process in which both the stress and strain increase. In the second segment, the SMA undergoes constrained recovery due to heating thereby deforming the beam. In order to obtain the initial conditions of the constrained recovery analysis, as discussed in the paper, the first segment is to be modeled.

Since the temperature is below the martensite finish temperature, the total martensite volume fraction remains constant; therefore, moduli $D(\xi_0)$ and $\Omega(\xi_0)$ are also constants. Thus, the constitutive equation of the SMA is written as

$$\sigma - \sigma_0 = D(\xi_0)(\varepsilon - \varepsilon_0) + \Omega(\xi_0)(\xi_s - \xi_{s0}) \tag{A2}$$

where the subscript 0 indicates the values corresponding to the undeformed configuration of the beam without the external load. Due to the external load *P*, the strain in the SMA is a function of the induced stress, as discussed in the previous paragraph. Following the phase kinetics stated in Eqs. (22c)–(22e) of Ref. [13], the volume fraction of the stress induced martensite can be obtained as $\xi_s = \xi_s(\sigma, T)$. It should be noted that ξ_s changes only if the induced stress is higher than the critical stress (σ_s^{cr}) required for detwinning. Equation (A2) is solved using Newton–Raphson method starting from an initial guess for the stress. Finally, the stress, strain, and ξ_s are obtained, which are used as the initial conditions for the constrained recovery.

With varying offset, the initial stress, strain, and ξ_s also vary affecting the final end deflection. The final value of the end deflection includes the initial negative deflection of the beam due to the load *P* and is calculated as $y_e = \bar{y}_e + \bar{\bar{y}}_e$, where the symbols are explained in Fig. 2(*a*).

References

[1] Liang, C., and Rogers, C. A., 1992, "Design of Shape Memory Alloy Actuators," ASME J. Mech. Des., **114**(2), pp. 223–230.
[2] Elahinia, M. H., and Ashrafiuon, H., 2002, "Non-Linear Control of a Shape Memory Alloy Actuated Manipulator," Trans. ASME, J. Vib. Acoust., **124**(4), pp. 566–575.
[3] Simpson, J. C., and Boller, C., 2008, "Design and Performance of a Shape Memory Alloy Reinforced Composite Aerodynamic Profile," Smart Mater. Struct., **17**(2), p. 025028.
[4] Bundhoo, V., Haslam, E., Birch, B., and Park, E. J., 2009, "A Shape Memory Alloy-Based Tendon-Driven Actuation System for Biomimetic Artificial Fingers, Part I: Design and Evaluation," Robotica, **27**, pp. 131–146.
[5] Banerjee, A., Bhattacharya, B., and Mallik, A. K., 2009, "Forward and Inverse Analyses of Two Link Compliant Mechanism," Mech. Mach. Theory, **44**(2), pp. 369–381.
[6] Chaudhry, Z., and Rogers, C. A., 1991, "Bending and Shape Control of Beams Using SMA Actuators," J. Intell. Mater. Syst. Struct., **2**(4), pp. 581–602.
[7] Brinson, L. C., Huang, M. S., Boller, C., and Brand, W., 1997, "Analysis of Controlled Beam Deflections Using SMA Wires," J. Intell. Mater. Syst. Struct., **8**(1), pp. 12–25.
[8] Funakubo, H., 1987, *Shape Memory Alloys*, Gordon and Breach, New York.
[9] Otsuka, K., and Wayman, C. M., 1998, *Shape Memory Materials*, Cambridge University Press, Cambridge.
[10] Tanaka, K., 1986, "A Thermomechanical Sketch for Shape Memory Effect: One-Dimensional Tensile Behavior," Res. Mech., **18**, pp. 251–263.
[11] DeCastro, J., Melcher, K. J., Noebe, R. D., and Gaydosh, D. J., 2007, "Development of a Numerical Model for High-Temperature Shape Memory Alloys," Smart Mater. Struct., **16**(6), pp. 2080–2090.
[12] Liang, C., and Rogers, C. A., 1990, "One Dimensional Thermomechanical Constitutive Relations for Shape Memory Materials," J. Intell. Mater. Syst. Struct., **1**, pp. 207–234.
[13] Brinson, L. C., 1993, "One-Dimensional Constitutive Behavior of Shape Memory Alloys: Thermomechanical Derivation With Non-Constant Material Functions and Redefined Martensite Internal Variable," J. Intell. Mater. Syst. Struct., **4**, pp. 229–242.
[14] Seelecke, S., and Müller, I., 2004, "Shape Memory Alloy Actuators in Smart Structures: Modeling and Simulation," Appl. Mech. Rev., **57**(1), pp. 23–46.